Jonapá-Hernández *et al.*
J Mater. Sci: Mater Eng. (2025) 20:83
https://doi.org/10.1186/s40712-025-00282-z

Journal of Materials Science: Materials in Engineering

ORIGINAL PAPER

Open Access

Cytotoxic effect of zinc oxide phytonanoparticles and *Bonellia macrocarpa* (Cav.) B. Stahl & Källersjö extract on breast cancer cell lines

Fermín Jonapá-Hernández[1,2], Nadia Judith Jacobo-Herrera[2], Beatriz del Carmen Couder-García[3], Joaquín Adolfo Montes-Molina[1], Federico Antonio Gutiérrez-Miceli[1], Eduardo Pérez-Arteaga[2] and María Celina Luján-Hidalgo[1*]

Abstract

This study focused on the synthesis of zinc oxide (ZnO) phytonanoparticles (PNPs) using *Bonellia macrocarpa* root extract and the evaluation of their cytotoxic activity in three cancer cell lines and the non-tumor control HaCaT cells. The PNPs were characterized using UV–Vis spectrophotometry, Fourier-transform infrared spectroscopy (FT-IR), particle analyzer, and scanning electron microscopy (SEM). The cytotoxic activity of ZnO PNPs was evaluated in the breast cancer cell lines MDA-MB-468, MDA-MB-231, and MCF-7. The results demonstrated a significant antiproliferative effect, particularly in the MDA-MB-468 cell line with an IC_{50} of 34 ppm, along with increased selectivity for this cell line compared to the crude extract and the reference drug, doxorubicin. Furthermore, the PNPs also reduced both the formation and size of tumor cell colonies and suppressed cell migration in the MDA-MB-468 line. These effects indicate a significant impact on the growth and spread of cancer cells. Moreover, PNPs successfully internalized into the cancer cells and induced a significantly higher overproduction of reactive oxygen species (ROS) compared to doxorubicin and the crude extract from *B. macrocarpa* roots. Finally, PNPs were observed to induce apoptosis in MDA-MB-468 cells, suggesting activation of programmed cell death pathways. The synthesis of PNPs offers an alternative for obtaining nanoscale structures with significant potential to reduce the progression of breast cancer. This approach may complement and enhance existing therapies for this disease.

Keywords Apoptosis, *Bonellia macrocarpa*, Breast cancer, Green synthesis, Nanomaterials, Phytonanoparticles, Reactive oxygen species

*Correspondence:
María Celina Luján-Hidalgo
maria.lh@tuxtla.tecnm.mx
Full list of author information is available at the end of the article

Springer Open

© The Author(s) 2025. **Open Access** This article is licensed under a Creative Commons Attribution 4.0 International License, which permits use, sharing, adaptation, distribution and reproduction in any medium or format, as long as you give appropriate credit to the original author(s) and the source, provide a link to the Creative Commons licence, and indicate if changes were made. The images or other third party material in this article are included in the article's Creative Commons licence, unless indicated otherwise in a credit line to the material. If material is not included in the article's Creative Commons licence and your intended use is not permitted by statutory regulation or exceeds the permitted use, you will need to obtain permission directly from the copyright holder. To view a copy of this licence, visit http://creativecommons.org/licenses/by/4.0/.

Introduction

Breast cancer (BC) is one of the most prevalent malignancies affecting women worldwide, with significant incidence across various age groups. According to the World Health Organization (WHO 2021), one in 12 women may develop BC. Moreover, the Pan American Health Organization (PAHO) reports a high incidence of breast cancer in Latin America and the Caribbean for the coming years.

Nanoparticles (NPs) in medicine have emerged as a promising tool for cancer diagnosis and treatment (FDA 2019; Sakahashi et al. 2022). NPs offer significant advantages over conventional therapies, enabling more precise and effective drug delivery while minimizing side effects (Raj et al. 2019). The versatility of NPs in drug delivery allows them to be designed for targeted therapy in various cancer types (Chandana et al. 2024), considering factors such as the acidity of the microenvironment and interactions with intra- or extracellular proteins (Jwa-Min Nam et al. 2003), or the incorporation of drugs into a nanometric matrix that controls their release to enhance pharmacodynamics (Roghaieh et al. 2024).

Various studies have reported that zinc oxide nanoparticles exhibit antiproliferative activity in a range of cancer cell lines, including human neuroblastoma (Kim et al. 2015), epidermoid carcinoma (Khan et al. 2021), cervical cancer (Lei et al. 2022), gastric cancer cell lines (Wujun et al. 2023), and breast cancer (Chaima et al. 2025). Recent efforts to integrate plant extracts and bioactive compounds of biological origin with anticancer properties into NPs formulations have expanded their applications. For instance, the crude extract and certain isolated metabolites, such as 1,3,5,6-tetrametoxi-8-metilnaftaleno, 3,5-dihidroxi-1,2,2-trimetilbenzociclobutao, 3-metoxi-5-octilfenol, 3-metoxi-2-metil-5-pentilfenol, protoprimulagenine, and bonediol obtained from the roots of *B. macrocarpa* demonstrated antimicrobial, cytotoxic, and antiproliferative properties in vitro (Caamal-Fuentes et al. 2011; Moo-Puc et al. 2015; Vila-Luna et al. 2017; Álvarez-Gutiérrez et al. 2019; Valencia-Chan et al. 2022). These bioactive properties of *B. macrocarpa* extracts, together with the presence of other metabolites such as phenols and flavonols with reducing capacity, make *B. macrocarpa* extract an excellent precursor for the synthesis of PNPs.

Green synthesis is an eco-friendly approach for the fabrication of metallic nanoparticles, utilizing plant-derived reducing and stabilizing agents due to the presence of phenolic compounds, among others, that have hydroxyl groups (Jayachandran et al. 2021; Jing et al. 2024; Chaima et al. 2025). It has also been reported that some bioactive properties of compounds present in these extracts are enhanced when incorporated into a nanometric matrix (Agarwal et al. 2017; Bandeira et al. 2020; Sadeghi et al. 2023). PNPs synthesized in this manner offer a novel approach to breast cancer treatment. Thus, this study evaluated the anticancer properties of ZnO PNPs synthesized from the crude extract of *B. macrocarpa*. Our findings indicate that these PNPs exhibit antiproliferative effects on the breast cancer cell lines MCF-7, MDA-MB-468, and MDA-MB-231. Additionally, we observed that PNPs inhibit colony formation, reduce cell migration, induce ROS production, and promote apoptosis-mediated cell death in MDA-MB-468 breast cancer cells.

Materials and methods

Plant material

The roots and leaves of *B. macrocarpa* were collected in the municipality of Tuxtla Gutiérrez, Chiapas, Mexico (16°43′39.2"N, 93°11′37.2"W) during the months of August and September 2020. The collected plants measured on average 60–90 cm from the base of the stem to the top of the plant canopy. The plant samples were washed with drinking water and dried at 50 °C. The dried roots were cut into fragments of ∼1 cm and crushed using an electric roller mill (SIEBTECHNIK TEMA). Finally, the plant material was ground (Basic Analytical Mill) until a fine dry powder was obtained. The plant extract was obtained by mixing the fine powder of *B. macrocarpa* roots or leaves with 96% methanol in a ratio of 1:50 g/mL. Fifty milliliters of methanol was added every 24 h, and the extraction was kept under constant agitation at room temperature and in darkness. The methanolic extract was filtered with filter paper (20–25 µm) using a vacuum. The leaves and roots were extracted to determine which tissues of *B. macrocarpa* contained the highest concentration of bonediol, a metabolite with biological activity in cancer cell lines that may also contribute to the formation of PNPs. Subsequently, the extract was concentrated with a rotary evaporator at 45 °C (Ruiz-Ramírez et al. 2018), recovered with distilled water, and lyophilized for storage in darkness at 4 °C. The plant extracts were characterized based on the total phenol content using the Folin-Ciocalteu reagent (Blainski et al. 2013), the content of flavones and flavonols (Chang et al. 2002), and the bonediol content quantified by high-performance liquid chromatography (Ruiz-Ramírez et al. 2018).

Synthesis and characterization of zinc oxide phytonanoparticles with *B. macrocarpa*

The synthesis of the PNPs was carried out according to the protocols of Velázquez-Gamboa et al. (2020) and Jonapá-Hernández et al. (2020) with modifications. One gram of the dry *B. macrocarpa* extract was resuspended in 75 mL of a methanol–water solution at a 1:3 ratio (v/v), then mixed with 150 mL of a 0.2 M zinc sulfate solution

for 20 min water bath at 60 °C with constant stirring of 1000 ± 100 rpm. Then, 225 mL of 0.1 M NaOH was added and maintained for another 20 min at 60 °C in the water bath at a constant stirring of 1000 ± 100 rpm. These synthesis conditions were obtained from the standardization of the synthesis method depending on the volume, concentrations of the solutions, and the reaction time to obtain the greatest amount of PNPs. The PNP colloidal solution was centrifuged at 4500 rpm for 15 min, and the precipitate was washed eight times, alternating four times with 15 mL 96% methanol and four times with 15 mL distilled water in 50 mL centrifuge tubes. This is to remove impurities from the PNPs, such as unreacted metabolites and synthesis residues. Additionally, these by-products can be recovered and properly treated for reuse, enhancing the environmental sustainability of the PNP synthesis process. Finally, the precipitate was dried in an oven at 45 °C and ground with a mortar to obtain a fine powder. The formation of PNPs was confirmed and compared to the spectrum of the crude extract from *B. macrocarpa* roots using a BECKMAN COULTER DU 730 UV–Vis spectrophotometer and a Thermo Scientific NICOLET iS10 infrared spectrometer (FT-IR). Particle size distribution and *Z* potential were determined using a Litesizer 500 particle analyzer (Anton Paar). The shape and size of the PNPs in powder form were observed through scanning electron microscopy (SEM) FE-SEM JSM-7100 F.

Cell line culture

The MCF-7, MDA-MB-468, and MDA-MB-231 breast cancer cell lines, as well as the non-tumoral keratinocyte HaCaT cell line, were obtained from the Biochemistry Unit of the National Institute of Medical Sciences and Nutrition Salvador Zubirán, Mexico City, México. The cells were cultured in 7 mL of DMEM-F12 culture medium (Gibco) supplemented with 10% inactivated fetal bovine serum (FBS) (B-Bio Classical) and 10 mL/L penicillin–streptomycin (Gibco). The cells were incubated at 37 °C with 5% CO_2.

Cytotoxicity assay

The sulforhodamine B method was used to evaluate the cytotoxic activity of the PNPs and to obtain the IC_{50} values (Orellana and Kasinski 2016). In 96-well plates, 1×10^4 cells per well were cultured with DMEM-F12 medium supplemented with 10% FBS and 10 mL/L penicillin–streptomycin. For the assays, the cells were incubated for 24 h at 37 °C with 5% CO_2. The culture medium was then removed and 200 µL of fresh medium supplemented with 2% FBS and PNP in a concentration range of 10 to 70 µg/mL was added, evaluating every 10 µg/mL and the incubation continued for 48 h. The median inhibitory concentration (IC_{50}) values were obtained using a non linear regression analysis with the inhibitor vs. normalized response method in GraphPad Prism 7 software. The concentrations proposed here were previously standardized to obtain an IC_{50} value with a high correlation with the inhibitor vs. normalized response method. The selectivity index (SI) was determined for the cancer cell lines compared to the non-tumoral HaCaT keratinocyte cell line. The selectivity index was calculated using Eq. 1 (Indrayanto et al. 2020).

$$SI = \frac{IC_{50}\ no\ tumor\ cells}{IC_{50}\ tumor\ cells} \quad (1)$$

Internalization of the PNPs

To determine the internalization of the PNPs in cancer cells in vitro, MDA-MB-468 cells were cultured in 6-well plates at a density of 5×10^5 cells/well with 4 mL of DMEM-F12 medium supplemented with 10% FBS and 1% penicillin–streptomycin. For this assay, the cells were incubated for 24 h at 37 °C with 5% CO_2. The culture medium was then removed, and 4 mL of fresh medium supplemented with 2% FBS and 17 ppm (IC_{25}) of PNPs were added. The plates were incubated for another 24 h. Afterward, the medium was removed, and the cells were harvested with trypsin. The cell suspension was centrifuged at 1500 rpm for 5 min. The precipitated cells were washed with Sörensen buffer pH 7.4, 0.2 M, resuspending and centrifuging three times consecutively. Finally, the cells were fixed by resuspending the pellet in 10 mL of glutaraldehyde. MDA-MB-468 cells untreated were the control observed with a transmission electron microscope (TEM) (Tecnai Spirit BioTwin, FEI, Hillsboro, OR, USA). Using the arithmetic IC_{25}, we ensured that most cells treated with PNPs did not exhibit severe damage, allowing them to recover after buffer washing and fixation with glutaraldehyde. This enabled us to retain a sufficient number of cells to observe internalization and subsequent PNP-cell interaction phenomena using TEM.

Effect of the PNPs on colony formation

In 6-well plates, 1×10^3 MDA-MB-468 cells were cultured in DMEM-F12 medium supplemented with 10% FBS and 10 mL/L penicillin–streptomycin. The cells were incubated for 72 h at 37 °C with 5% CO_2. After incubation, the culture medium was removed and replaced with fresh medium containing 2% FBS and the IC_{50} was obtained for each treatment in the cytotoxicity assay. The cells were incubated for 10 days under the same conditions. Afterward, the colonies were fixed with 500 µL of trichloroacetic acid (TCA), stained with crystal violet, and the number of colonies was counted (Lei et al. 2022). Additionally, macroscopic morphology was observed

with a Nikon Eclipse TS100 microscope and a ProgRes CT3 JENOPTIK camera.

Evaluation of cell migration inhibition

The effect of the PNPs on cell migration was evaluated using the wound healing assay. In 6-well plates, 1×10^6 MDA-MB-468 and HaCaT cells were cultured in DMEM-F12 medium supplemented with 10% FBS and 10 mL/L penicillin–streptomycin. For the assays, the cells were incubated for 24 h at 37 °C with 5% CO_2. Then, the medium was removed, the cells were washed with PBS, and a wound was made on the cell monolayer, followed by another wash with PBS. Fresh medium with 2% FBS supplemented with 10 ppm PNPs was then added. The wound closure was observed using a Nikon Eclipse TS100 microscope and a ProgRes CT3 JENOPTIK camera at 24, 48, and 72 h. Untreated cells were used as controls to evaluate migration changes induced by the application of PNPs in normal HaCaT cells and tumor MDA-MB-468 cells. The images were analyzed using the ImageJ software.

Induction of reactive oxygen species

To evaluate the increase in ROS, 1×10^5 MDA-MB-468 cells per well were cultured in 96-well plates for 24 h using DMEM/F12 medium supplemented with 10% FBS. After 24 h of incubation, the medium was replaced with fresh medium supplemented with 2% FBS and the different treatments (PNPs 34 ppm, crude extract 8.7 ppm, and doxorubicin 1.5 ppm). The plates were cultured for 24 h with each treatment. After the treatments, the cells were washed with PBS and were then stained with 10 µM DHE in a serum-free medium for 30 min at 37 °C in the dark. ROS production was monitored every 5 s for 1.5 h by using a Varioskan microplate reader (Thermo Fisher Scientific Waltham, MA, USA) $\lambda em = 605$ nm and $\lambda ex = 518$ nm. The DHE fluorescence was normalized as a percentage of the fluorescence intensity from non-treated living cells (Liu et al. 2014; Rodríguez-Enríquez et al. 2019).

Cellular apoptosis (annexin V/PI staining)

Triple-negative breast cancer MDA-MB-468 cells were cultured at a density of 2.5×10^4 cells per well in 6-well plates using DMEM/F12 medium supplemented with 10% FBS and 10 mL/L penicillin–streptomycin. The cells were incubated for 24 h at 37 °C with 5% CO_2. Next, the medium was replaced with a fresh medium containing 2% FBS, and the IC_{50} of the PNPs was evaluated. UV light radiation was applied for 10 min as a positive control. The cells were incubated for 24 and 48 h. Then, they were stained with annexin V and PI fluorochromes from the BioLegend kit, following the manufacturer's instructions. The samples were acquired using a BD ACCURI C6 Plus flow cytometer at the National Institute of Respiratory Diseases of México (INER).

Statistical analysis

The results were analyzed using a means comparison test with Tukey's honestly significant difference (HSD) procedure, with a $p \leq 0.5$ (Statgraphics Centurion XV 1.1). The IC_{50} analyzes were performed using the dose–response test in the GraphPad Prism program. All experiments were performed in triplicate.

Results

Quantification of phenols, flavones, flavonols, and bonediol in *B. macrocarpa* extracts

Table 1 shows the content of phenols, flavones, flavonols, and bonediol present in the leaves and roots of *B. macrocarpa*. The concentration of total phenols in the leaf extract was 6.79 mg GAE/g of dry leaves, while the concentration in the root extract was 4.85 mg GAE/g of dry root. The content of flavone and flavonol in the leaves was 2.90 mg QE/g of dry leaves, whereas in root extract showed a concentration of 1.85 mg QE/g of dry roots. The bonediol content in the root extract was 68 mg bonediol/g of dry tissue. This compound has been reported to exhibit cytotoxic activity against cancer cell lines, which is why the root extract was used for PNP synthesis.

Characterization of ZnO and *B. macrocarpa* PNPs

The successful synthesis of the PNPs was indicated by a distinctive color change from brown to white at the end of the synthesis. In the UV–Vis absorption spectrum of the colloidal nanoparticle solution, a peak with maximum absorbance at 330 nm was observed (Fig. 1C), characteristic of ZnO nanoparticles. FT-IR analysis of the *B. macrocarpa* root extract revealed bands in the 3600–2800 cm^{-1} range, corresponding to the stretching vibrations of O–H and C–H bonds. A prominent band was also observed around 1600 cm^{-1} attributed to the C= O stretching vibration, characteristic of organic compounds present in the extract, such as flavonoids, phenolic acids, aldehydes, and catechols, among others

Table 1 Phenol, flavones, flavonols, and bonediol content of *B. macrocarpa* extracts

Metabolite	Leaf	Root	HSD
Total phenols (mg GAE/g*)	6.79 ± 0.135 A	4.85 ± 0.32 B	0.55
Flavones and flavonols (mg QE/g*)	2.90 ± 0.1 A	1.85 ± 0.25 B	0.48
Bonediol (mg B/g*)	NA	68.0 ± 1.82	

Equal letters between rows have no statistically significant difference, $p \leq 0.5$

HSD honestly significant difference, *GAE* gallic acid equivalent, *QE* quercetin equivalent, *B* bonediol, *g** gram of dry plant material, *NA* no detected

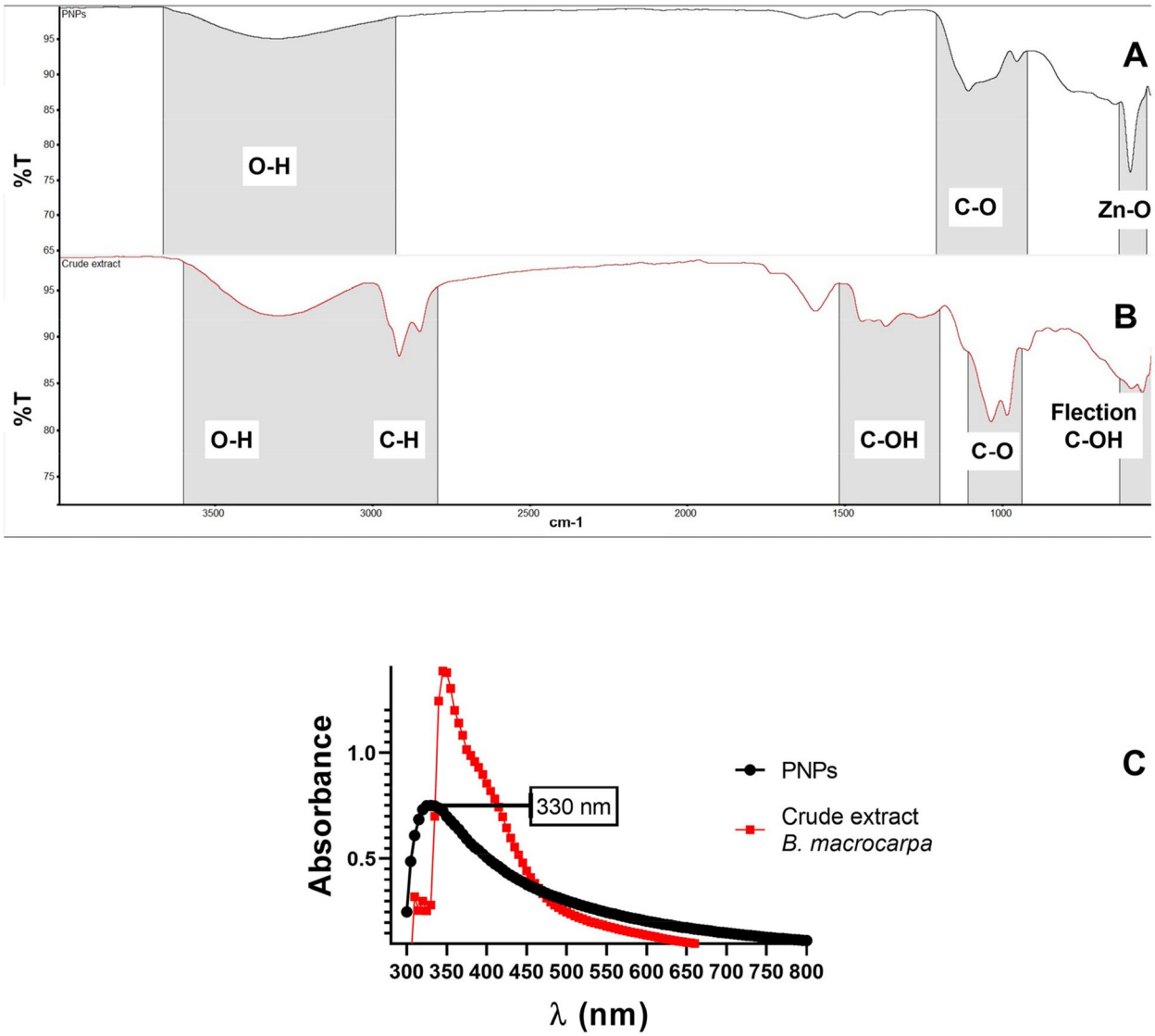


Fig. 1 FT-IR spectral scans. **A** ZnO PNPs. **B** Extract *B. macrocarpa* roots. **C** UV–Vis absorption spectrum where the maximum absorbance peak of the ZnO PNPs with *B. macrocarpa* extract is indicated

(Fig. 1B). The presence of these same analytical signals in the FT-IR spectrum of the PNPs confirmed the incorporation of the *B. macrocarpa* metabolites during the synthesis of the PNPs. The band observed at 600 cm^{-1} in the PNP spectrum corresponds to the stretching vibrations of the Zn–O bond (Fig. 1A). This signal coincides with that reported by various authors who have described that metal oxides typically exhibit absorption bands in the infrared region below 1000 cm^{-1} (Jayachandran et al. 2021; Gnanasekaran et al. 2024). Size distribution analysis of the PNPs in an ultrasound-dispersed medium indicated that 95.2% of the particles had a diameter of 5.72 nm and possessed a negative surface charge, with a *Z* potential of 0.5 mV and PDI 10.91 (Fig. 2A–C). SEM analyses showed that the PNPs formed macrostructures at the micrometer scale (Fig. 2D,E), as well as substructures in flake form at the nanometer scale (Fig. 2F,G). Proper characterization of the PNPs is crucial for further standardization of the treatment.

Assays of cytotoxicity and index of selectivity of PNPs in breast cancer cells and HaCaT

Table 2 resumes the IC_{50} values obtained for the PNPs, the crude extract, and the doxorubicin in three breast cancer cells lines and HaCaT. The response was dose-dependent across all evaluated cell lines (Fig. 3).

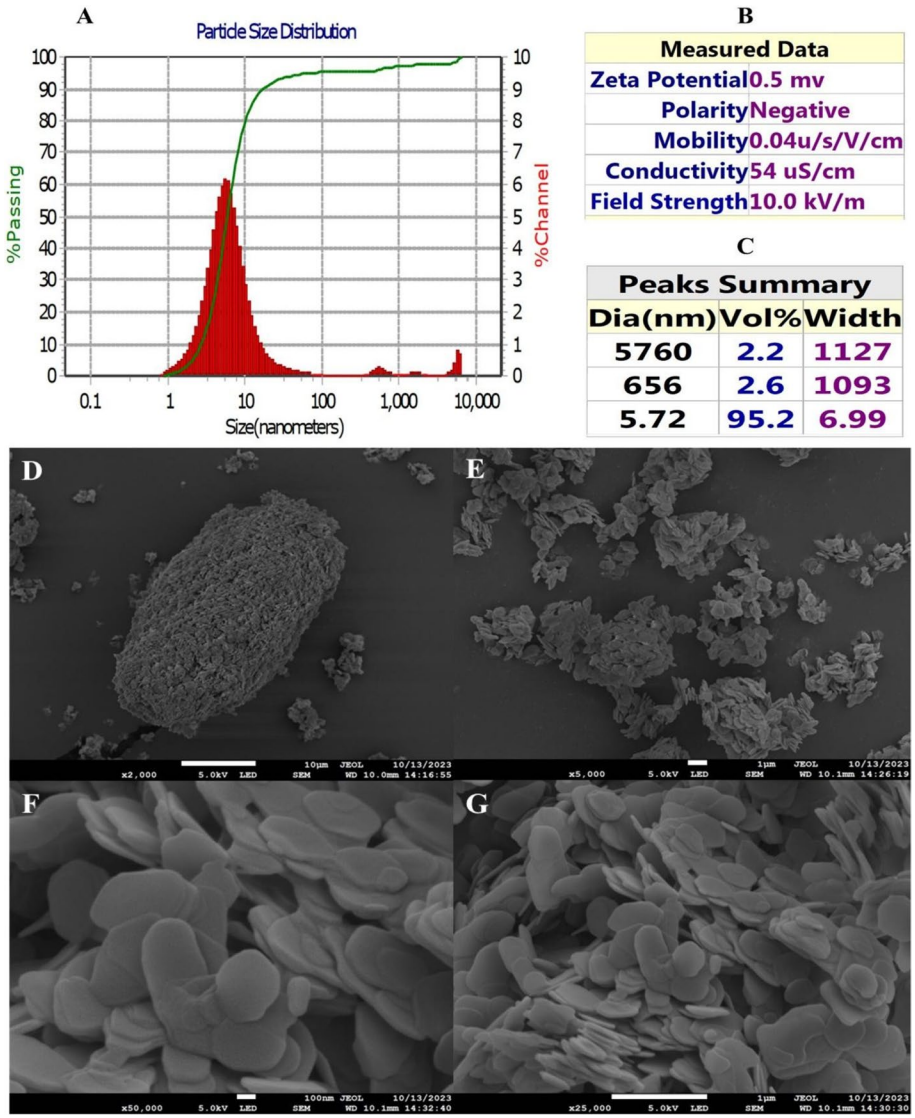


Fig. 2 **A** Size distribution graph. **B** Physicochemical properties of the PNPs. **C** Table summarizing major peaks with percentages and sizes. **D**, **E** Macrostructures formed by the PNPs seen by SEM. **F**, **G** Substructures formed by the dry PNPs seen by SEM

Table 2 IC_{50} values obtained for breast cancer cell lines and HaCaT

	IC_{50} (ppm)				
Treatment	**HaCaT**	**MDA-MB-468**	**MDA-MB-231**	**MCF-7**	**HSD**
PNPs	30.12 ± 1.53 A	34.07 ± 1.6 AB	39.14 ± 3.3 BC	44.13 ± 3.8 C	7.295
Crude extract of *B. macrocarpa*	3.11 ± o.32 A	8.68 ± 1.43 B	11.13 ± 1.52 BC	14.13 ± 1.3 C	3.303
Doxorubicin	0.30 ± 0.26 A	1.25 ± 0.20 B	3.45 ± 0.34 C	0.75 ± 0.18 AB	0.673

Equal uppercase letters in the same row do not have statistically significant differences, $p \leq 0.5$

HSD honestly significant difference

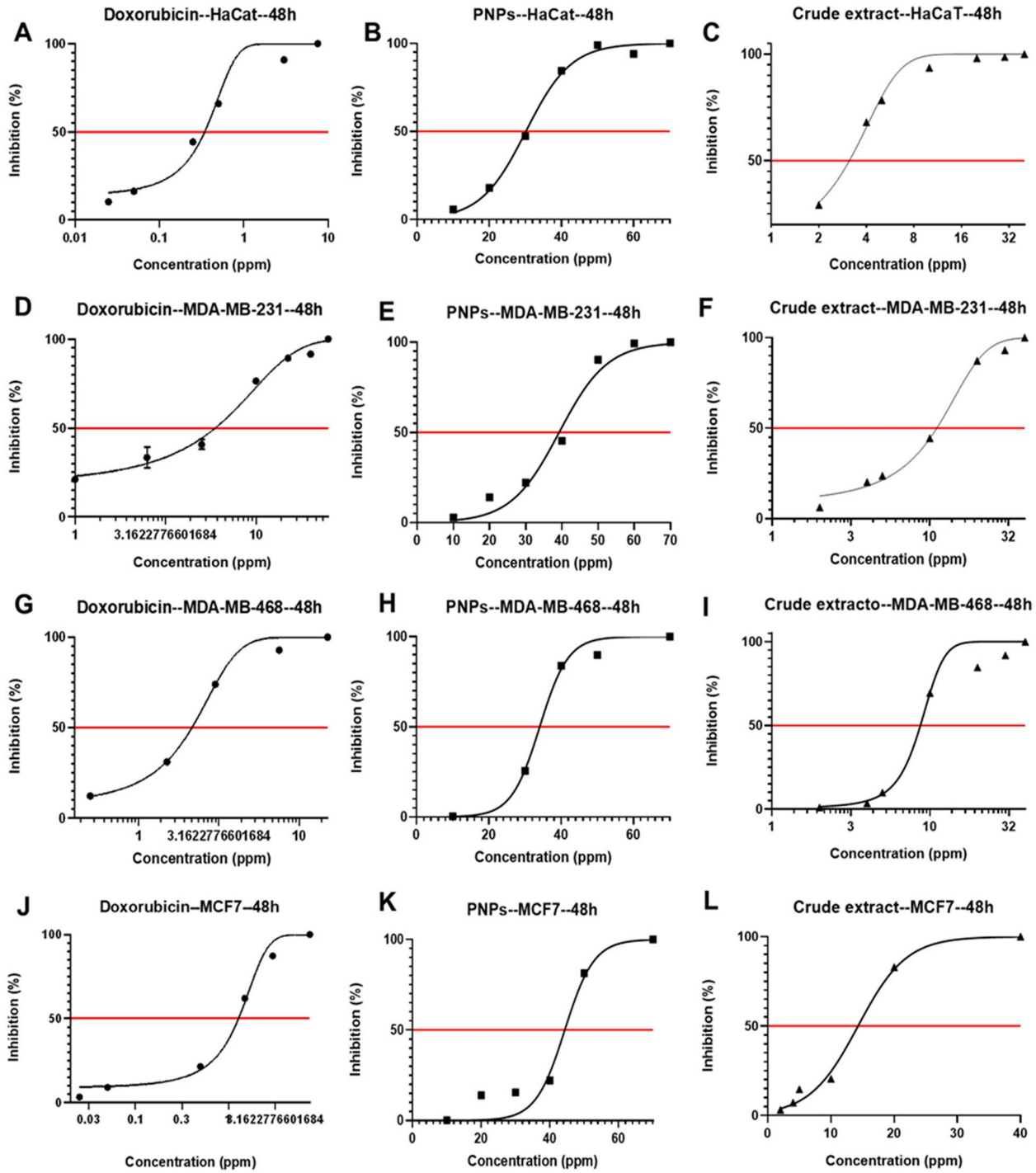


Fig. 3 Graphs showing the inhibition of cell proliferation induced by doxorubicin, PNP, and the crude root extract of *B. macrocarpa* after 48 h of exposure using the sulforhodamine B colorimetric method. The graphs were generated using the GraphPad Prism 8.0 statistical program and the normalized dose–response inhibitor model. Panels **A**, **B**, and **C** represent the effects on the HaCaT cell line when exposed to doxorubicin, PNP, and crude root extract, respectively. Panels **D**, **E**, and **F** represent the corresponding effects on the MDA-MB-231 cell line, while panels **G**, **H**, and **I** illustrate the effects on the MDA-MB-468 cell line. Finally, panels **J**, **K**, and **L** show the effects on the MCF-7 cell line when treated with doxorubicin, PNP, and crude root extract, respectively

According to the IC_{50} values of the three breast cancer cell lines, the MDA-MB-468 presented the lower number, exhibiting an IC_{50} of 34.07. However, the crude extract showed a cytotoxic effect with better values in all cell lines in comparison to PNPs. Such a result could be due to the synergy of the variety of compounds, increasing cell death. Notwithstanding, the PNPs are in the range of cytotoxicity activity for cancer cells. The index of selectivity (Table 3) indicates the more sensitive cancer cell line exposed to treatment (Indrayanto et al. 2020). Our results showed that MDA-MB-468 was the most sensitive culture, the reason to be used for internalization assays, colony formation tests, scratch assays, ROS production quantification, and apoptosis induction analysis followed by PNP application.

The cytotoxicity and index of selectivity tests were two key evaluations to determine the concentration of the treatments used for the next experiments. Based on the obtained IC_{50} values, the concentrations used in cell migration experiments, colony formation, internalization, ROS production, and cell apoptosis were standardized according to the specific observations required and the limitations of the cell model. However, for experiments such as cell migration, a concentration lower than the IC_{50} was selected.

Internalization of the PNPs into MDA-MB-468 cells

The PNPs successfully internalized into MDA-MB-468 cells, with electron-dense structures observed within the cells (Fig. 4). These structures were primarily located at the periphery of the cells (Fig. 4B,F). Notably, electron-dense structures were observed only in cells exposed to PNPs and were absent in the control cells (Fig. 4G,H). Additionally, PNPs were detected inside structures resembling phagosomes (Fig. 4D,E), and evidence of cellular membrane disruption was observed (Fig. 4C). This experiment allowed us to be sure the PNPs passed through the cell membrane by microscopy images.

Table 3 Index of selectivity of treatments towards breast cancer cells

Treatment	MDA-MB-468	MDA-MB-231	MCF-7
PNPs	0.88 ± 0.04 G	0.76 ± 0.06 FG	0.68 ± 0.05 EF
Crude extract of *B. macrocarpa*	0.35 ± 0.06 CD	0.27 ± 0.03 BC	0.22 ± 0.02 BC
Doxorubicin	0.22 ± 0.16 A	0.084 ± 0.064 A	0.36 ± 0.23BC
HSD: 0.167			

The same letters have no statistically significant difference, $p \leq 0.5$

HSD honestly significant difference

Inhibition of colony formation

This technique permitted us to visualize the effects of the PNPs on proliferation and the inhibition in the formation of new colonies. It also provided insight into the efficacy of the PNPs, crude extract, and doxorubicin with respect to exposure time. The colonies formed by MDA-MB-468 cells after 10 days of different treatments and exhibited morphometric variances mainly in size and cell count. The number of colonies formed by MDA-MB-468 cells decreased by 39.7% after treatment with PNPs. In contrast, the drug doxorubicin reduced the number of colonies by 56.8% in MDA-MB-468 (Fig. 5). Notably, the crude extract of *B. macrocarpa* showed no significant effect on the inhibition of MDA-MB-468 cell colony formation (Table 4). A reduction in the number of colonies after treatment with PNPs and doxorubicin is related to cell proliferation, the cells might be reducing their proliferation rate in a time and dose-dependent behavior.

Cell migration inhibition

Cell migration was assessed using a wound healing assay in both MDA-MB-468 cells and the no-tumor cells, HaCaT. Considering that the control for evaluating PNPs in tumor cells consists of MB-468 cells without PNPs, wound closure represents 100% of the cellular migration in these cells. Upon PNP application, wound closure was inhibited by 69.53% at 72 h (Fig. 6A,C). In the non-tumoral HaCaT cells, the application of PNPs did not yield a statistically significant difference in wound closure, allowing for complete closure. It is noteworthy that the proliferation and migration rates varied among cell lines, with the non-tumoral line covering more than 90% of the wound area at 48 h. In summary, the PNPs are able to halt cell migration at 24 h, an effect that persisted until 72 h. Inhibition of migration is another important target of anticancer drugs since this phenomenon is related to metastasis, one of the main concerns in cancer patients.

(See figure on next page.)

Fig. 4 Internalization of PNPs in MDA-MB-468 cells after 24 h of exposure. A transmission electron microscope (TEM) (Tecnai Spirit BioTwin, FEI, Hillsboro, OR, USA) was used for imaging. **A** Control cells (not treated). **B** Cells containing internalized PNPs (red arrows point to the PNPs), size 1 micron. **C** Magnified view of image B (500 microns), highlighting the interaction of PNPs with mitochondria (blue arrows point to mitochondria). **D** Cells treated with PNPs, showing the presence of vacuole-like structures and internalized PNPs (yellow circles enclose the vacuole). **E** Enhanced presence of vacuole-like structures containing PNPs (red arrows), magnification 500 microns. **F** PNPs localized along the periphery of cell membranes (red arrows). **G**, **H** Comparative images of untreated MDA-MB-468 cells and cells treated with PNPs after 24 h of exposure, respectively

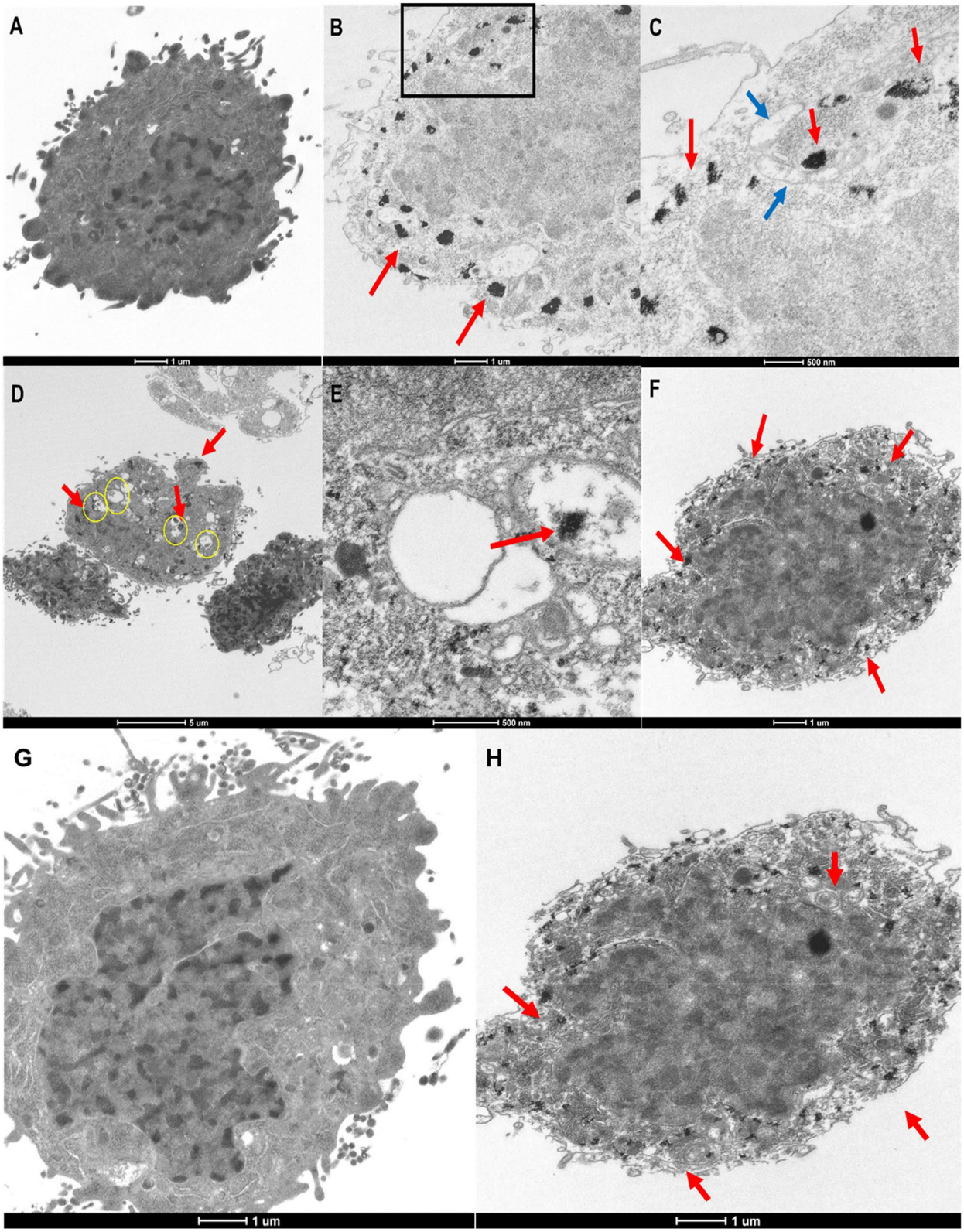


Fig. 4 (See legend on previous page.)

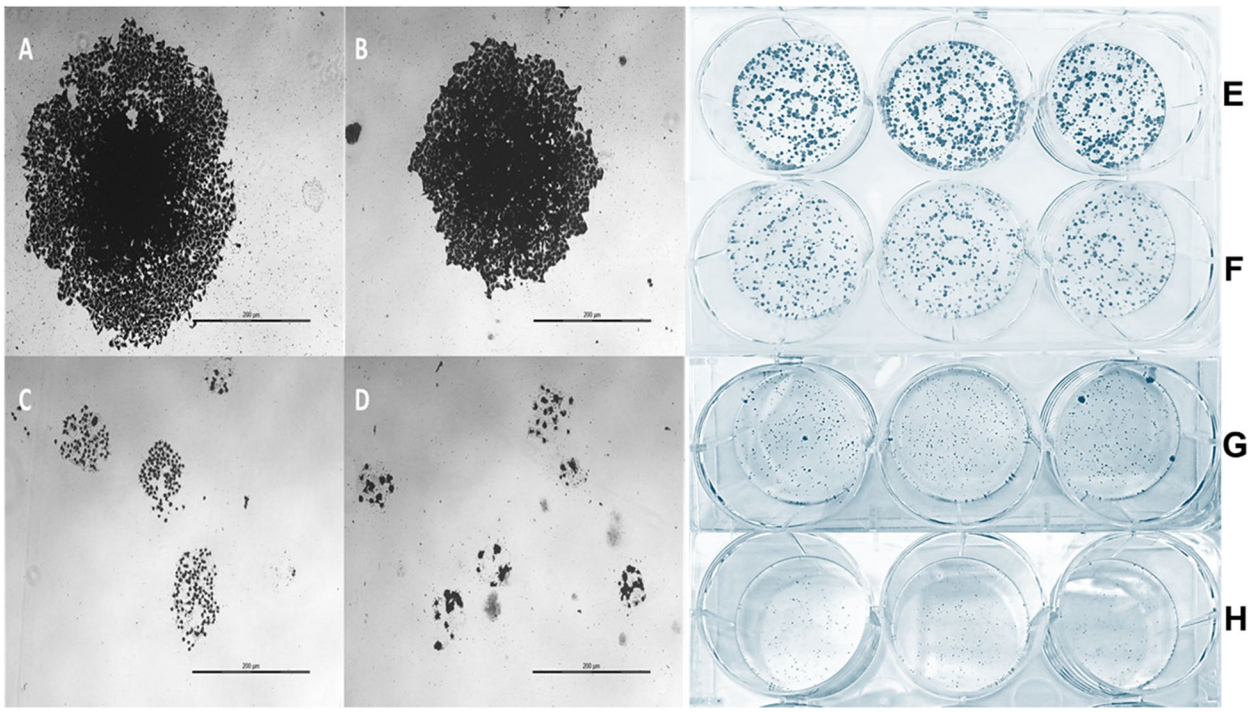


Fig. 5 MDA-MB468 cell colonies. **A**, **E** Untreated cells. **B**, **F** Colony of cells treated with the crude extract. **C**, **G** Colonies of cells treated with PNPs. **D**, **H** Colonies of cells treated with doxorubicin. Scale bar 200 µm. Macroscopic morphology was observed using a Nikon Eclipse TS100 microscope and a ProgRes CT3 JENOPTIK camera

Induction of reactive oxygen species (ROS) and apoptosis

Figure 7 depicts the increment of ROS levels in MDA-MB468 cells treated with PNPs compared to the untreated cells after 24 h of exposure. Also, the effect of the PNPs was higher than that generated by doxorubicin and the crude extract of *B. macrocarpa* in MDA-MB-468 (Fig. 7E).

On the other hand, we wanted to find out whether PNPs promote apoptosis in MDA-MB-468 as a cell death mechanism of action. Thus, a double dye with annexin V and PI was performed (see Methodology Sect. 2.9). Figures 8B and G visualize that 80% of the cells treated with PNPs at a concentration of 34 ppm for 24 h were in the early stage of apoptosis and presented a time-dependent behavior (quadrant right low). Contrary, after 48 h of treatment, the population of cells in early apoptosis decreased to 28% and cells in late apoptosis increased to 66%. Likewise occurred with the positive control ultraviolet (UV) radiation (Fig. 8C,F). Such results indicate the antioxidant activity of the PNPs by the rise of the ROS levels in MDA-MB-468 cells, which might be implicated in the pro-apoptosis effect provoking cell death.

Table 4 Number of MDA-MB-468 colonies

Treatment	No. of colonies
Control	248.50 ± 35.8 C
PNPs	149.83 ± 7.16 B
Crude extract of *B. macrocarpa*	239.0 ± 13.3 C
Doxorubicin	107.33 ± 12.54 A
HSD: 31.25	

The same letters have no statistically significant difference, $p \leq 0.5$

HSD honestly significant difference

Discussion

The root extract of *Bonellia macrocarpa* contains a diverse array of specialized metabolites, including phenols, flavones, flavonols, and bonediol—a catechol-type compound of particular interest due to its previously reported antiproliferative activity against cancer cell lines (Caamal-Fuentes et al., 2011; Moo-Puc et al. 2015; Valencia-Chan et al. 2022). The bonediol content in the root extract obtained for the synthesis of PNPs was higher than that reported by Ruiz-Ramírez et al. (2018), who found 2.78 mg bonediol/g of dry transformed roots, and by Castro-Martínez et al. (2022), who obtained 49.57 mg bonediol/g of callus. All these bioactive molecules play a crucial role in PNP synthesis, particularly in the formation of metal–phenolic networks (MPNs) through coordination bonds, resulting in stable complexes (Tang et al. 2025). Additionally, they contribute to the

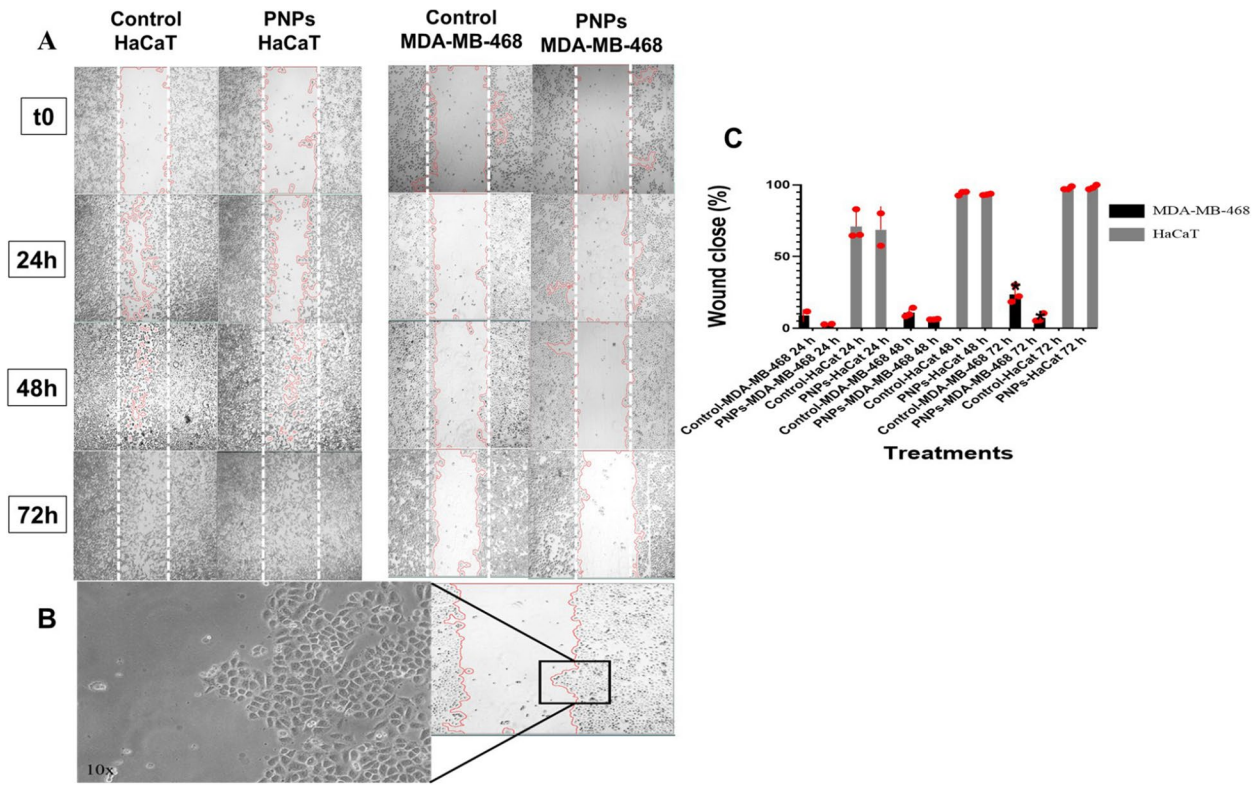


Fig. 6 **A** Images of wound closure in HaCaT and MDA-MB-468 cells with and without exposure to PNPs at time zero, 24, 48, and 72 h. The cell lines were treated with 10 ppm (IC_{20}). **B** Magnification of MDA-MB-468 cell structures at 24 h without PNPs. **C** Percentage of wound closure in MDA-MB-468 and HaCaT cell monolayers at 24, 48, and 72 h with and without PNPs. The bar with (**) indicates a statistical difference from its control, $*p \leq 0.5$

functionalization of metal and metal oxide PNPs, such as ZnO, by modifying their surface. This surface modification enhances their dispersion in aqueous media, improves biocompatibility, and imparts additional functionalities, such as antioxidant activity and selective affinity for specific cellular receptors.

FT-IR analysis of the PNPs revealed characteristic stretching bands corresponding to O–H, C–H, and C = O bonds. These signals indicate the presence of organic compounds from the *B. macrocarpa* root extract—such as flavonoids, phenols, and potentially bonediol—on the surface of the PNPs. The reported maximum absorption wavelength for zinc oxide nanoparticles typically ranges from approximately 330 to 380 nm. Factors influencing the shift in the absorption band include nanoparticle size, shape, crystalline structure, the dispersion medium, and the presence of surface coatings or organic compounds. In Fig. 1, both the crude extract and the plant-mediated nanoparticles (PNPs) exhibit similar absorption peaks (~ 330 nm), suggesting that the PNPs optical properties may be influenced by metabolites present in the extract. Nevertheless, X-ray diffraction (XRD) analysis is crucial to confirm the crystalline structure and chemical composition of the nanoparticles. While UV–Vis spectroscopy, FT-IR, DLS, and SEM provided valuable characterization data, XRD would offer complementary structural insights essential for a more comprehensive understanding of the nanoparticles.

Regarding cytotoxic activity, the plant extract, phytonanoparticles (PNPs), and the drug may have their effects on cancer cells through different mechanisms of action. Consequently, their cytotoxicity is observed at different concentration ranges, which were determined through preliminary assays aimed at identifying the appropriate range for calculating the IC_{50} of each treatment.

The assay to evaluate PNP internalization into cells was conducted using the IC_{25} (17 ppm) to prevent nanoparticle agglomeration during analysis, minimize cellular damage, and facilitate the observation of interactions with the cell membrane.

The cell migration assay was carried out using a concentration of 10 ppm, selected based on the IC_{50} determined in the cytotoxicity assay. High concentrations can induce cell death, potentially compromising the accurate interpretation of migration behavior. Therefore, sub-cytotoxic concentrations were used to ensure

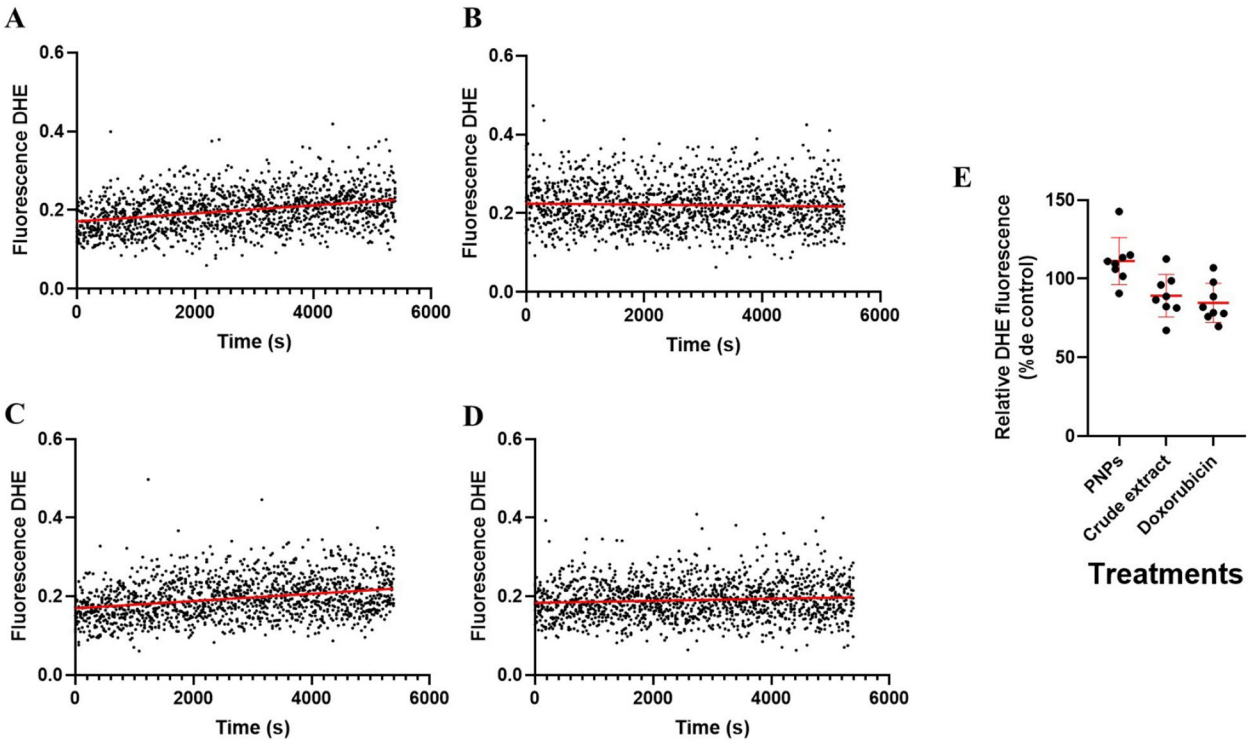


Fig. 7 The trend of ROS production in the MDA-MB-468 cell line under different treatments after 24 h of exposure. **A** Control (untreated cells). **B** MDA-MB-468 cells treated with PNPs (34 ppm IC_{50}). **C** MDA-MB-468 cells treated with crude extract (8.68 ppm IC_{50}). **D** MDA-MB-468 cells treated with doxorubicin (1.25 ppm IC_{50}). **E** Relative percentage of ROS levels compared to control cells

that any observed effects on migration were attributable to changes in cellular behavior rather than cytotoxicity.

In contrast, the evaluations of colony formation, reactive oxygen species (ROS) production, and apoptosis induction were performed using the IC_{50} concentration of the PNPs.

The PNPs demonstrated cytotoxic activity against three different breast cancer cells (MDA-MB-468, MDA-MB-231, and MCF-7) (Fig. 3J, K, and L). Several authors reported that size is a crucial factor in the cytotoxicity of NPs, facilitating interaction and entry into tumor cells through mechanisms such as passive diffusion, ion channels, or pinocytosis (Feltis et al. 2012; Condello et al. 2016; Yao et al. 2020; Jabir et al. 2021). In this context, the small hydrodynamic size of the PNPs, approximately 6 nm (Fig. 2C), may favor internalization. In our model, doxorubicin exhibited the highest cytotoxicity against tumor cells when compared to other treatments. However, when evaluating the selectivity index, despite doxorubicin being more cytotoxic, the PNPs displayed superior selectivity towards BC cell lines. Calderón-Montaño et al. (2021) suggested that the lack of selectivity associated with doxorubicin necessitates reducing drug dosage to concentrations that do not harm non-tumor cells, ultimately leading to low efficacy in patients with metastasis.

PNPs contain metabolites from *B. macrocarpa* root extract that can act synergistically with zinc oxide molecules to induce cytotoxicity in breast cancer cell lines. Zinc sulfate and oxide of zinc are classified as "Generally Recognized As Safe" (GRAS) by the U.S. Food and Drug Administration (FDA), while zinc is an essential micronutrient that plays various structural and enzymatic roles in the human body (Nriagu et al. 2019a). The reported safety of the zinc as a micronutrient could be related to the PNP's low cytotoxicity in non-tumor HaCaT cells compared to doxorubicin and the crude extract of *B. macrocarpa* roots. Moo-Puc et al. (2015) reported bonediol as partially affinity-estradiol receptors and cytotoxicity action in cells lacking receptors, with its mechanism of action being attributed to oxidative stress.

Additionally, the increased levels of ROS in MDA-MB-468 cells (Fig. 7B) may result from dysregulation of cellular homeostasis due to the release of zinc ions from the PNPs. It was also noted that the trend in ROS levels in cells treated with PNPs was decreasing (Fig. 7B). This decrease may be attributed to the high cytotoxicity of the PNPs before 24 h of exposure, resulting in reduced ROS levels at the time of quantification due to induced

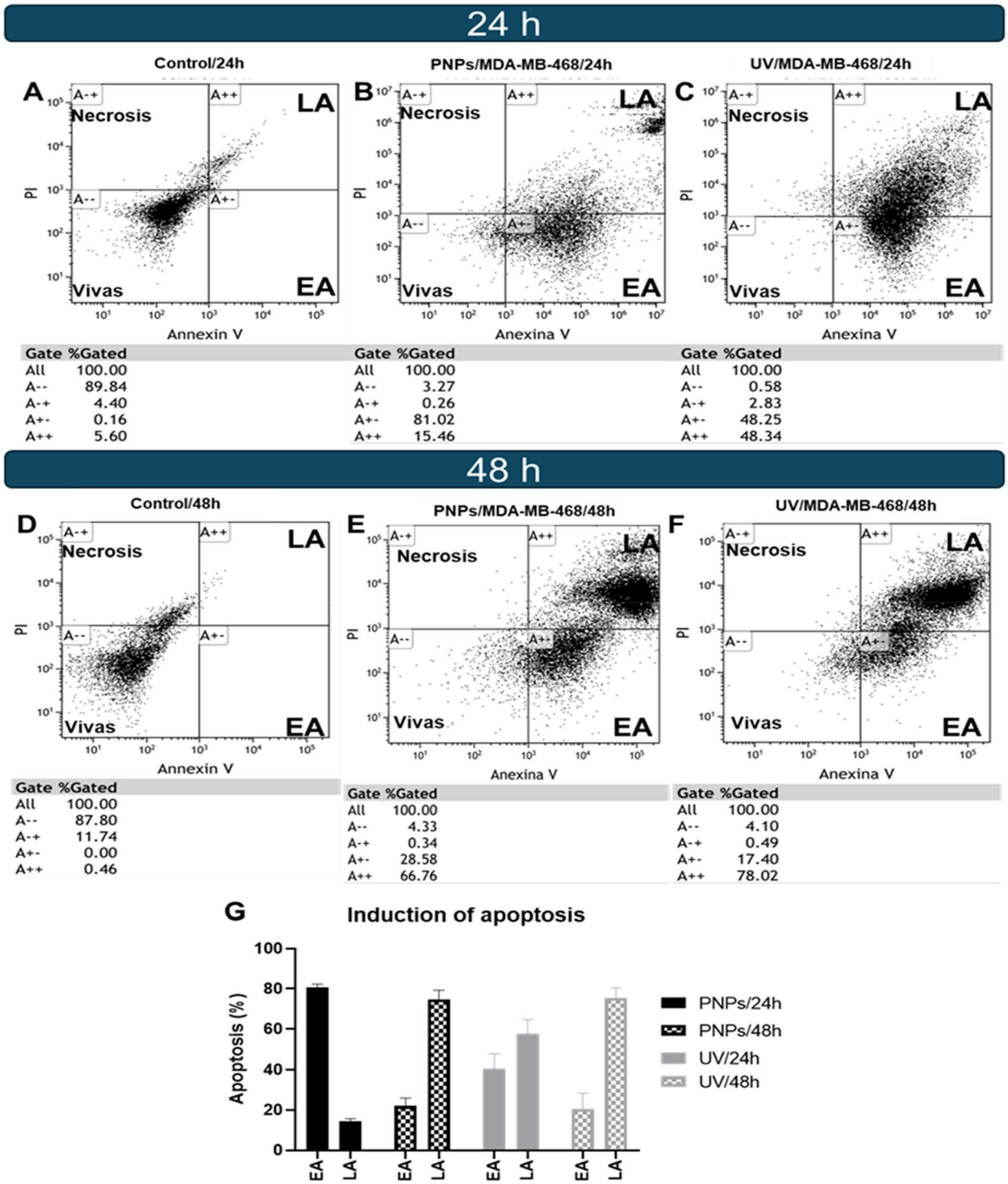


Fig. 8 Induction of apoptosis in the MDA-MB-468 cell line. **A** Untreated control cells after 24 h. **B** Apoptosis induction by PNPs after 24 h. **C** UV-induced apoptosis after 24 h. **D** Untreated control cells after 48 h. **E** Apoptosis induction by PNPs after 48 h. **F** UV-induced apoptosis after 48 h. **G** Percentage of apoptosis induction at the early stage (EA) and late stage (LA) during different exposure times of the treatments

cell death in tumor cells. Consequently, biological activity and ROS production decreased, leading to a downward trend in ROS levels during quantification compared to the crude extract of *B. macrocarpa* and doxorubicin (Fig. 7).

When assessing the clonogenicity of PNPs in comparison to the crude extract and doxorubicin in MDA-MB-468 tumor cells, a significant reduction in the number of colonies was observed (Table 4). Those colonies treated with PNPs (Fig. 5C,G) or doxorubicin (Fig. 5D,H) showed changes in size, shape, and cell density. The colonies treated with PNPs were smaller than those observed with the crude extract and control, exhibiting a response comparable to that induced by doxorubicin. The extract itself demonstrated no statistically significant difference in the number of colonies compared to the negative control. However, the colonies resulting from the extract were smaller than the control colonies (Fig. 5A, B, E, and F). This phenomenon could be due to the fact that metabolites or bioactive compounds in the plant extract, such as polyphenols or bonediol, can bind to proteins present in fetal bovine serum in the culture medium. This binding can alter the bioavailability of the compounds and reduce their ability to interact with cancer cells (Papadopoulou and Frazier 2004). This underscores the goal of synthesizing PNPs with these plant extracts, as metabolites incorporated into nanometric matrices could remain in the human body for extended periods, combined with a gradual release of these components, potentially enhancing pharmaceutical utilization (Younas et al. 2023; Nandhini et al. 2024).

The wound healing assay showed that PNPs reduce the migration of selected breast cancer cells (Fig. 6A). After 24 h of exposure, MDA-MB-468 cells exhibited collective movement structures (Fig. 6B), indicative of cell migration (Spano et al. 2012). However, in the presence

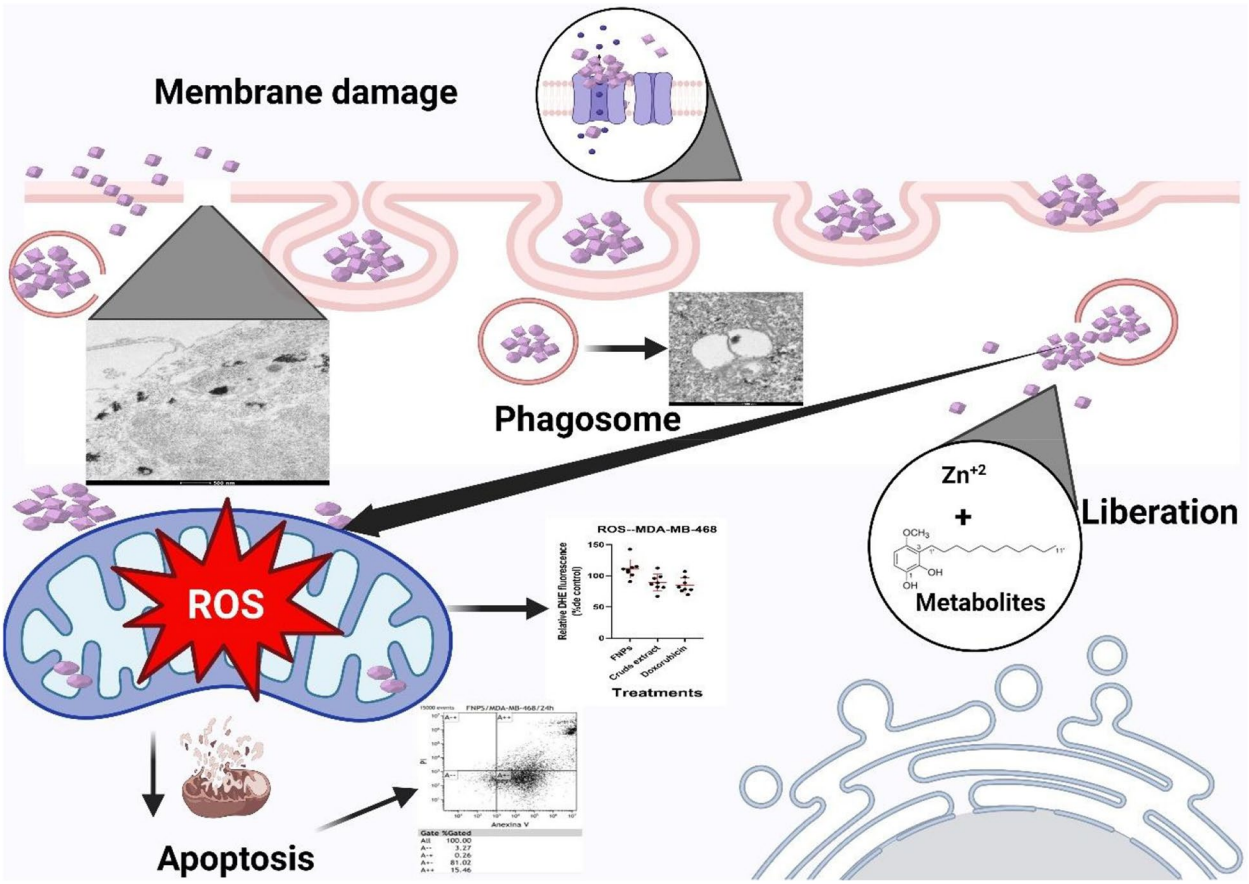


Fig. 9 Summary of the mechanism of action of nanoparticles (PNPs) in MDA-MB-468 cells. PNPs are internalized via endocytosis and encapsulated in phagosomes within the cell. During this process, membrane damage is observed, which may facilitate the controlled release of bioactive metabolites and Zn^{2+}. Oxidative stress is induced through the production of reactive oxygen species (ROS), compromising mitochondrial function and triggering apoptosis. Transmission electron microscopy (TEM) images provide evidence of PNP interaction and internalization within the cells, as well as their effects on cellular morphology. Additionally, flow cytometry and relative DHE fluorescence data confirm the increase in ROS levels in response to PNP treatment

of PNPs at concentrations below the IC_{50}, the formation of such structures was inhibited. Additionally, it was found that PNPs did not significantly affect the migration of healthy cells. These findings highlight the selectivity action of PNPs on tumor cells. Although PNPs at concentrations below the IC_{50} did not significantly reduce cell proliferation, they did reduce the migration of these cells, suggesting that at low concentrations, PNPs influence mechanisms associated with motility and migration in tumor cells.

Our results indicate that PNPs induce apoptosis in MDA-MB-468 cells. However, the percentages of early and late-stage apoptosis were time-dependent, with an increase in late apoptosis observed 48 h after treatment compared to 24 h. This pattern was similar to that seen with UV light radiation. PNPs may induce apoptosis after internalization into the cells, resulting in damage to cellular membranes, including those of the mitochondria, as shown in Fig. 4C, where PNPs are seen in contact with the mitochondria (Fig. 9). Condello et al. (2016) noted that NPs can be attracted to cell membranes due to their polarity, leading to mechanical damage, the overproduction of reactive oxygen species, or the release of pro-apoptotic proteins such as cytochrome C. This protein is part of the apoptosome in the cytosol, triggering the caspase signaling cascade that culminates in tumor cell apoptosis.

Conclusion

The PNPs synthesized from the crude root extract of *B. macrocarpa* and zinc oxide effectively reduced the proliferation of triple-negative BC cells (MDA-MB-468 and MDA-MB-231) as well as the estrogen receptor-positive MCF-7 cell line, primarily through the induction of apoptosis. Furthermore, they diminished the number of tumor colonies and inhibited cell migration in MDA-MB-468. Overall, the PNPs exhibited greater selectivity toward cancer cells compared to their precursor, the *B. macrocarpa* root extract, and doxorubicin, suggesting they may serve as an alternative to the development of new BC treatments. Further studies should be performed to complete the antitumor understanding of the PNPs in BC cells.

Abbreviations

BC	Breast cancer
CDMX	Ciudad de México
FBS	Fetal bovine serum
FDA	Food and Drug Administration
PNPs	Phytonanoparticles
FT-IR	Fourier transform infrared spectroscopy
GAE	Gallic acid equivalent
GRAS	Generally Recognized As Safe
HSD	Honestly significant difference
IC_{50}	Inhibitory concentration 50%
INER	National Institute of Respiratory Diseases of México
SI	Selectivity Index
NPs	Nanoparticles
PAHO	Pan American Health Organization
ppm	Parts per million
QE	Quercetin equivalent
TCA	Trichloroacetic acid
UV	Ultraviolet
WHO	World Health Organization

Acknowledgements

The authors are grateful to the Secretaría de Ciencias, Humanidades, Tecnología e Innovación (SECIHTI), for providing financial support to Fermín Jonapá-Hernández in conducting this research. We are also thankful to the Instituto Nacional de Tecnología de México and Instituto Nacional de Ciencias Médicas y Nutrición Salvador Zubirán for providing their facilities for the research.

Authors' contributions

All of the authors contributed to the design and implementation of the research, to the analysis of the results, and to the writing of the manuscript.

Funding

Tecnológico Nacional de México/Instituto Tecnológico de Tuxtla Gutiérrez, Instituto Nacional de Ciencias Médicas y Nutrición Salvador Zubirán, Secretaría de Ciencias,Humanidades,Tecnología e Innovación

Data Availability

The datasets used and/or analysed during the current study are available from the corresponding author on reasonable request.

Declarations

Competing interests

The authors declared no conflicts of interest.

Author details

[1]Departamento de Ingeniería Bioquímica, Tecnológico Nacional de México, Instituto Tecnológico de Tuxtla Gutiérrez, Carretera Panamericana Km 1080, Tuxtla Gutiérrez, Chiapas C.P. 29050, México. [2]Unidad de Bioquímica Guillermo Soberón Acevedo, Instituto Nacional de Ciencias Médicas y Nutrición Salvador Zubirán, Vasco de Quiroga 15, Belisario Domínguez Sec. 16, Tlalpan, CDMX C.P. 14080, México. [3]SECIHTI-Centro de Investigación y Asistencia en Tecnología y Diseño del Estado de Jalisco, Subsede Sureste, Parque Científico y Tecnológico de Yucatán, Tablaje Catastral 31264, Mérida C.P. 97302, México.

Received: 31 October 2024 Accepted: 23 April 2025
Published online: 20 June 2025

References

Agarwal H, Venkat KS, Rajeshkumar S (2017) A review on green synthesis of zinc oxide nanoparticles – An eco-friendly approach. Resour-Efficient Technol (3):406-413. https://doi.org/10.1016/j.reffit.2017.03.002.

Álvarez-Gutiérrez PE, Ruiz-Ramirez LA, Godoy-Hernández G del C, Gutiérrez-Miceli FA, (2019) Bonediol production in *Bonellia macrocarpa* hairy root culture. Plant Cell Tissue Differ Sec Metabolites 1–21. https://doi.org/10.1007/978-3-030-11253-0_24-1

Bandeira Marina; Giovanela Marcelo; Roesch-Ely Mariana; Devine Declan M. and da Silva Crespo, Janaina, (2020). Green synthesis of zinc oxide nanoparticles: a review of the synthesis methodology and mechanism of formation. Sustainable Chemistry and Pharmacy, 15. https://doi.org/10.1016/j.scp.2020.100223.

Blainski A, Lopes GC, de Mello JC (2013) Application and analysis of the folin ciocalteu method for the determination of the total phenolic content from *Limonium brasiliense* L. Molecules 18(6):6852–6865. https://doi.org/10.3390/molecules18066852

Calderón-Montaño JM, Martínez-Sánchez SM, Jiménez-González V, Burgos-Morón E, Guillén-Mancina E, Jiménez-Alonso JJ, Díaz-Ortega P, García

F, Aparicio A, López-Lázaro M (2021) Detection of selective anticancer activity of 65 plant extracts collected in Western Andalusia, Spain. *Plants* 10(10). https://doi.org/10.3390/plants10102193.

Chaima Benine, Djahra Ali Boutlelis, Laiche Ammar Touhami, Elhafnaoui Lanez, Djilani Ghemam Amara, Gatrane Rim, Najjaa Hanen, Wafa Zahnit and Mohammed Messaoudi, (2025). Green synthesis, characterization, antioxidant, interaction with DNA/BSA, and investigation of cytotoxicity against MCF-7 cancer cells of zinc oxide nanoparticles using *Hammada scoparia* (Pomel) Iljin extract. International Journal of Biological Macromolecules. (295). https://doi.org/10.1016/j.ijbiomac.2025.139709.

Chandana Surya, Ashoka Babu Vechham Lakshminarayana, Sameera Hammigi Ramesh, Selvaraj Kunjiappan, Panneerselvam Theivendren, A. Santhana Krishna Kumar, Damodar Nayak Ammunje, Parasuraman Pavadai. (2024). Advancements in breast cancer therapy: the promise of copper nanoparticles, Journal of Trace Elements in Medicine and Biology, 86. https://doi.org/10.1016/j.jtemb.2024.127526.

Chang C. C., Yang M. H., Wen, H. M. and Chern J.-C., (2002). Estimation of total flavonoid content in propolis by two complementary colorimetric methods. Journal of Food and Drug Analysis: 10. https://doi.org/10.38212/2224-6614.2748.

Condello M, De Berardis B, Ammendolia MG, Barone F, Condello G, Degan P, Meschini S (2016) ZnO nanoparticle tracking from uptake to genotoxic damage in human colon carcinoma cells. Toxicol in Vitro 35:169–179. https://doi.org/10.1016/j.tiv.2016.06.005

Caamal-Fuentes E, Torres-Tapia LW, Cedillo-Rivera Moo-Puc R, Peraza-Sánchez SR (2011) Bonediol, a newalkyl catechol from *Bonellia macrocarpa*. Phytochemistry Letters 4(3):345–347. https://doi.org/10.1016/j.phytol.2011.07.006

FDA. (2019). Nanotecnología / Nanotoxicología. 18/07/2023, de FDA Sitio web: https://www.fda.gov/medical-devices/cdrh-research-programs/nanotechnology nanotoxicology.

Feltis BN, OKeefe SJ, Harford AJ, Piva TJ, Turney TW, Wright PF (2012) Independent cytotoxic and inflammatory responses to zinc oxide nanoparticles in human monocytes and macrophages. Nanotoxicology 6(7):757-65. https://doi.org/10.3109/17435390.2011.620718.

Gnanasekaran R, Yuvaraj D, Koteswara Reddy G, Naveen Shangar S, Vijayakumar V, Iyyappan J (2024) Zinc oxide nanoparticles from leaf extract of *Eclipta prostrata*: biosynthesis and characterization towards potential agent against film forming bacteria in metal working fluids. Environmental Chemistry and Ecotoxicology 6:206–215. https://doi.org/10.1016/j.enceco.2024.06.001

Indrayanto G, Putra GS, Suhud F (2020) Validation of in-vitro bioassay methods: Application in herbal drug research. Profiles Drug Subst Excip Relat Methodol 46:273-307. https://doi.org/10.1016/bs.podrm.2020.07.005

Jabir MS, Hussien AA, Sulaiman GM, Yaseen NY, Dewir YH, Alwahibi MS, Soliman DA, Rizwana H (2021) Green synthesis of silver nanoparticles from *Eriobotrya japonica* extract: a promising approach against cancer cells proliferation, inflammation, allergic disorders and phagocytosis induction. Artif Cells Nanomed Biotechnol 49(1):48- 60. https://doi.org/10.1080/21691401.2020.1867152

Jayachandran A., T.R. A. and Nair A. S., (2021). Green synthesis and characterization of zinc oxide nanoparticles using *Cayratia pedata* leaf extract. Biochemistry and Biophysics Reports. 26. https://doi.org/10.1016/j.bbrep.2021.100995.

Jing Zhao, Yun-hui Hu, Shi-yong Zhou, Wei Li, Zheng Song, Qian Fan, Xia Liu, Xiang-rui Meng, Xian-huo Wang and Hui-lai Zhang, (2024). Evaluation of the anti-breast cancer properties of *Origanum majorana* aqueous extract green-mediated nanoparticles, Inorganic Chemistry Communications. 169. https://doi.org/10.1016/j.inoche.2024.113098.

Jonapá-Hernández Fermín, Gutiérrez-Miceli Federico, Santos-Espinosa Ana, Ruíz-Lau Nancy, Ruíz-Valdiviezo Victor, Valdez-Salas Benjamín, González-Mendoza Daniel, (2020). Foliar application of green nanoparticles in *Annona muricata* L. plants and their effects in physiological and biochemical parameters. Biocatalysis and Agricultural Biotechnology, 28. https://doi.org/10.1016/j.bcab.2020.101751.

Jwa-Min Nam C, Thaxton S, Mirkin CA (2003) Nanoparticle-based bio-bar codes for the ultrasensitive detection of proteins. Science 301:1884–1886. https://doi.org/10.1126/science.1088755

Kim JH, Jeong MS, Kim DY, Her S, Wie MB (2015) Zinc oxide nanoparticles induce lipoxygenase-mediated apoptosis and necrosis in human neuroblastoma SH-SY5Y cells. Neurochem. https://doi.org/10.1016/j.neuint.2015.09.002

Khan MJ, Ahmad A, Khan KMA, Siddiqui S (2021) Zinc oxide nanoparticle induces apoptosis in human epidermoid carcinoma cells through reactive oxygen species and DNA degradation. Biol Trace Elem Res 199:2172–2181. https://doi.org/10.1007/s12011-020-02323-4

Lei JY, Li SX, Feng Li, Hui Li, Lei YS (2022) Zinc oxide nanoparticles regulate the ferroptosis, proliferation, invasion and steaminess of cervical cancer by miR-506-3p/CD164 signaling. Cancer Nano 13:33. https://doi.org/10.1186/s12645-022-00134-x

Liu M, Ye J, Gao S, Fang W, Li H, Geng B, Zou J, Chen X, Chen S, Zhang L, Yue Z, Ma., Y., Gao H., Li Z. and Liu P. (2014) Salvianolic acid B protects cardiomyocytes from angiotensin II-induced hypertrophy via inhibition of PARP-1. Biochem Biophys Res Commun 444(3):346–353. https://doi.org/10.1016/j.bbrc.2014.01.045

Moo-Puc Rosa, Caamal-Fuentes Edgar, Peraza-Sánchez Sergio R., Slusarz Anna, Jackson Glenn, Drenkhahn Sara K. and Lubahn Dennis B., (2015). Antiproliferative and antiestrogenic activities of bonediol an alkyl catechol from *Bonellia macrocarpa*. BioMed Research International, 1–6. https://doi.org/10.1155/2015/847457.

Nandhini J, Karthikeyan E, Rajeshkumar S (2024) Green synthesis of zinc oxide nanoparticles: eco-friendly advancements for biomedical marvels. Resources Chemicals and Materials. https://doi.org/10.1016/j.recm.2024.05.001

Nriagu Jerome, (2019a). Zinc deficiency in human health. Encyclopedia of Environmental Health (Second Edition), 489–499. https://doi.org/10.1016/B978-0-12-409548-9.11433-2.

Orellana Esteban and Kasinski Andrea (2016). Sulforhodamine B (SRB) assay in cell culture to investigate cell proliferation. BIO-PROTOCOL, 6(21). https://doi.org/10.21769/BioProtoc.1984.

Papadopoulou A, y Frazier, R. A. (2004) Characterization of protein–polyphenol interactions. Trends in Food Science y Technology 15(3–4):186–190. https://doi.org/10.1016/j.tifs.2003.09.017

Raj S, Khurana S, Choudhari R, Kumar KK, Kamal MA, Garg N, Kumar D (2019) Specific targeting cancer cells with nanoparticles and drug delivery in cancer therapy. Semin Cancer Biol 69:166–177. https://doi.org/10.1016/j.semcancer.2019.11.002

Rodríguez-Enríquez S., Pacheco-Velázquez S.C., Marín-Hernández Á., Gallardo-Pérez J.C., Robledo-Cadena D.X., Hernández-Reséndiz I., García-García J.D., Belmont-Díaz J., López-Marure R., Hernández-Esquivel L., Sánchez-Thomas R. and Moreno-Sánchez R., (2019). Resveratrol inhibits cancer cell proliferation by impairing oxidative phosphorylation and inducing oxidative stress. Toxicol Appl Pharmacol. 65–77, https://doi.org/10.1016/j.taap.2019.03.008.

Roghaieh Holghoomi, Maria Hassan Kiani, Abbas Rahdar, Seyed Mehdi Hashemi, Luiz Fernando Romanholo Ferreira, Sonia Fathi-karkan, (2024). Nanoparticle-delivered gallic acid: a new frontier in cancer therapy. Journal of Drug Delivery Science and Technology, 101. https://doi.org/10.1016/j.jddst.2024.106129.

Ruiz-Ramírez LA, Godoy-Hernández G, Álvarez-Gutiérrez PE, Ruíz-Valdiviezo VM, Luján-Hidalgo MC, Avilés-Berzunza E, Gutiérrez-Miceli FA (2018) Protocol for bonediol production in *Bonellia macrocarpa* hairy root culture. Plant Cell Tissue Organ Cult. https://doi.org/10.1007/s11240-018-1403-z

Sadeghi Dousari Amin, Soheil Hosseininasab Seyed, Reza Akbarizadeh Majid, Naderifar and Naghmeh Satarzadeh Mahin, (2023). *Mentha pulegium* as a source of green synthesis of nanoparticles with antibacterial, antifungal, anticancer, and antioxidant applications. Scientia Horticulturae, 320. https://doi.org/10.1016/j.scienta.2023.112215.

Sakahashi Y, Higashisaka K, Isaka R, Izutani R, Seo J, Furuta A,Tsutsumi Y (2022) Silver nanoparticles suppress forskolin-induced syncytialization in BeWo cells. Nanotoxicology 16(9–10):883–894. https://doi.org/10.1080/17435390.2022.2162994

Spano D, Heck C, De Antonellis P, Christofori G, Zollo M (2012) Molecular networks that regulate cancer metastasis. Semin Cancer Bio 22(3):234–249. https://doi.org/10.1016/j.semcancer.2012.03.006

Tang Z, Huang Z, Huang Y, Huang M, Liu H, Du J, Jia B (2025) Nanomedicine's shining armor: understanding and leveraging the metal-phenolic networks. Journal Nanobiotechnology 23:158. https://doi.org/10.1186/s12951-025-03210-7

Valencia-Chan LS, Moreno-Lorenzana DL, Josué C-C, Chávez-Gónzalez MA, Peraza-Sánchez SR, Moo-Puc RE (2022) Evaluation of protoprimulagenin A

and bonediol isolated from *Bonellia macrocarpa* in myeloid leukemia cell lines. Rev Bras 32:651–656. https://doi.org/10.1007/s43450-022-00274-6

Velázquez-Gamboa MC, Rodríguez-Hernández L, Abud-Archila M, Gutiérrez-Miceli FA, González-Mendoza D, Valdez-Salas B, Luján-Hidalgo MC (2020) Agronomic Biofortification of *Stevia rebaudiana* with zinc oxide (ZnO) phytonanoparticles and antioxidant compounds. Sugar Tech 23:453–460. https://doi.org/10.1007/s12355-020-00897-w

Vila-Luna SE, Moo-Puc RE, Torres-Tapia LW, Peraza-Sánchez SR (2017) New metabolites with cytotoxic and antiproliferative activities isolated from *Bonellia macrocarpa*. Phytochem Lett 19:121–125. https://doi.org/10.1016/j.phytol.2016.12.016

WHO. (2021). CÁNCER. 03/03/2021, de OMS. Sitio web: https://www.who.int/es/news-room/fact-sheets/detail/cancer.

Wujun Du, Ke Feng, Cunji Li, Shengming Li, Zain Ul Abidin, Hua Yin and Shensi Chen, (2023). Controlled synthesis of zinc oxide nanoparticles through flame spray pyrolysis and evaluation of their anticancer effects against gastric cancer cell. Arabian Journal of Chemistry, 16(10). https://doi.org/10.1016/j.arabjc. 2023.105192.

Yao Yihan, Zhou Yunxiang, Liu Lihong, Xu Yanyan, Chen Qiang, Wang Yali, Wu Shijie, Deng Yongchuan, Zhang Jianmin and Shao Anwen, (2020). Nanoparticle-based drug delivery in cancer therapy and its role in overcoming drug resistance. Frontiers in Molecular Biosciences. 7. https://doi.org/10.3389/fmolb.2020.00193.

Younas Zohaib, Zia Ur Rehman Mashwani, Ilyas Ahmad, Maarij Khan, Shah Zaman and Laraib Sawati Sohail, (2023). Mechanistic approaches to the application of nano-zinc in the poultry and biomedical industries: a comprehensive review of future perspectives and challenges. Molecules. 28(3). https://doi.org/10.3390/molecules28031064.

Publisher's Note

Springer Nature remains neutral with regard to jurisdictional claims in published maps and institutional affiliations.